Research Square

Preprints are preliminary reports that have not undergone peer review.
They should not be considered conclusive, used to inform clinical practice,
or referenced by the media as validated information.

Design And Analysis of 2-Dof Flexure Based Micromanipulator With Bridge Type Amplifier

Abdullah Al Fuad
Chittagong University of Engineering and Technology
M.A. Shadab Siddiqui
mashadab002@gmail.com

Chittagong University of Engineering and Technology
Dr. Syed Mohammad Hossain
University of Dhaka

Research Article

Keywords: Flexure-based micromanipulator, Mechanism optimization, Finite element analysis, Precision positioning application

Posted Date: January 1st, 2024

DOI: https://doi.org/10.21203/rs.3.rs-3807533/v1

License: This work is licensed under a Creative Commons Attribution 4.0 International License.
Read Full License

Additional Declarations: No competing interests reported.

Design And Analysis of 2-Dof Flexure Based Micromanipulator With Bridge Type Amplifier

Abdullah Al Fuad[a], M.A.Shadab Siddiqui[a]*, Dr. Syed Mohammod Hossain[b]

[a]*Department of Mechanical Engineering, Chittagong University of Engineering and Technology, Chattogram, Bangladesh.*

[b]*Department of physics, Dhaka University, Dhaka, Bangladesh.*

Abstract:

In this study, a novel 2-DOF flexure-based micromanipulator for applications requiring precise positioning is designed and analyzed. The micromanipulator has a bridge-type amplification mechanism and an in-plane XY micropositioning stage that make it very stiff and accurate. The findings of the mechanism's examination using finite element analysis (FEA) and simulations indicate that the workspace range is 22.2 mm and the natural frequency is 150 Hz. The study also looks into how the characteristics of the material affect the mechanism's performance. The micromanipulator is fabricated using Al 7075-T6, demonstrating a displacement amplification ratio of 9.68. Geometrical modeling is established. The result shows that a compliant parallel micromanipulator's workspace is obtained at $\pm$191.81 μm× $\pm$192.41 μm. The amplification ratio is 6.77 analytically and 6.19 computationally. The natural frequency was found to be 2134 Hz and validated analytically. The study's findings demonstrate the potential of flexure-based mechanisms for achieving precise positioning in micro-scale applications. Overall, the study shows the promise of flexure-based mechanisms for applications requiring precise positioning, representing a substantial leap in the field of micro-manipulation.

Keywords: Flexure-based micromanipulator, Mechanism optimization, Finite element analysis, Precision positioning application.

1. INTRODUCTION:

Flexure-based compliant manipulators offer advantages over traditional joint mechanisms due to having no backlash, no friction, and vacuum compatibility as motion and force are transmitted through elastic deformations [1]. This offers more rigidity and precision than traditional revolute, prismatic, or spherical joints. Due to their small size and capacity for large strokes, compliant manipulators are used in high-precision applications like optical fiber alignment, atomic force microscopy, microsurgery, and micromanipulation [1][2].

Their structure can be categorized as serial or parallel, with serial designs establishing 1-DOF mechanisms and parallel designs providing high accuracy, stiffness and load capacity [2]. Decoupled designs simplify control while isolation protects actuators from parasitic motions that reduce accuracy [3]. Micromanipulators using flexure hinges can achieve ultra-high precision for various applications by relying on smooth, elastic motion instead of friction-producing mechanical joints [4].

*Corresponding author.

Email address: mashadab002@gmail.com (M.A. Shadab Siddiqui)

Piezoelectric actuators enable nanoscale precision but have limited stroke, while voice coils provide greater motion at the cost of force ability [5]. Even a three-pound concrete ball could be thrown more than 200 yards by this machine [6]. Degrees of Constraint (DOC) are used to describe constrained directions, whereas Degrees of Freedom (DOF) are used to describe unrestrained directions. In Fig 1 conventional constraint elements have been shown.

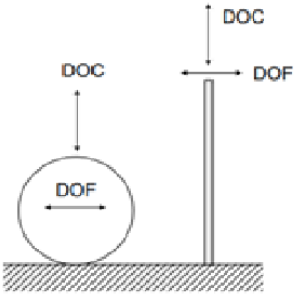


Fig. 1: Example of conventional constraint elements [7].

At a general level, the flexure hinges can be divided into two categories: primitive flexure hinges and complex flexure hinges [9]. Overall, flexure manipulators leverage elastic deformations for frictionless precision manipulation. The stiffness matrix is K, and the compliance matrix is C. C and K are opposites. The right-angle flexure compliance matrix is represented as follows:

$$C=\begin{bmatrix} \frac{l}{Ebt} & 0 & 0 & 0 & 0 & 0 \\ 0 & \frac{4l^3}{3Ebt^3}+\frac{l}{Gbt} & 0 & 0 & 0 & \frac{6l^2}{Ebt^3} \\ 0 & 0 & \frac{4l^3}{3Eb^3t}+\frac{l}{Gbt} & 0 & \frac{-6l}{Eb^3t} & 0 \\ 0 & 0 & 0 & \frac{l}{Gk_2bt^3} & 0 & 0 \\ 0 & 0 & \frac{-6l^2}{Eb^3t} & 0 & \frac{12l}{Eb^3t} & 0 \\ 0 & \frac{6l^2}{Ebt^3} & 0 & 0 & 0 & \frac{12l}{Ebt^3} \end{bmatrix} \quad [10]$$

Stiffness matrix, $K=C^{-1}$

Development of micromanipulators involves systematic testing and evaluation for applications from industrial robots to microsurgery tools.[11-15] Compliant mechanisms provide advantages like high stiffness, accuracy through eliminating friction and backlash, and lower cost compared to traditional joints.[16-20] However, limitations include inability to achieve continuous motion and stress concentration risks.[21-23] Previous studies on flexure-based manipulators analyzed parasitic motion reduction, increased stiffness, decoupling and workspace enhancement through optimization, but achieved output displacement did not match expected values in some cases.[24-30] New designs incorporated methods like topology optimization, hysteresis modeling, and asymmetric amplification to maximize performance metrics.[31-36] Most utilized piezoelectric actuation but voice coils provide greater motion range at the cost of force ability. Research gaps included parasitic motion limitations in multi-DOF designs and load-induced displacement losses. This study aims to address such issues through developing a new 2-DOF parallel flexure micromanipulator with voice coil actuation, conducting static, dynamic and stress analyses by simulation to characterize workspace, stiffness, natural frequency and displacement amplification for robotic applications requiring precision positioning.[38]

This study aims to design a novel 2-DOF flexure-based micromanipulator with objectives including achieving translational X-Y motion, revealing the workspace, gaining high resonant frequency, minimizing parasitic motion, investigating dynamics via simulation, determining amplification ratio

analytically and by FEA, and characterizing flexure stiffness. Challenges arise from the non-linear mechanics of complex flexure combinations, fatigue issues, and limited achievable motion. Compliant mechanisms offer advantages over traditional joints such as high stiffness, accuracy by eliminating friction and backlash, lower cost and better efficiency. However, limitations include inability to achieve continuous motion, stress concentration risks, and wear due to cyclic loading. The scope of this research is to develop a mechanism enabling precise positioning by exploiting flexure mechanics while overcoming joint-based shortcomings like errors and friction, providing a contribution to future micro-manipulation applications.

2. METHODOLOGY:

The study designed and analyzed a 2-DOF monolithic parallel flexure-based micromanipulator with high frequency using simulation methods. The 3D model was created using CAD software, and structural analysis was performed to calculate workspace range, rotational stiffness, output stiffness, and displacement. Stress analysis and dynamic modelling were used to investigate the structure's stability. Fig. 2 illustrates the CAD model of the micromanipulator which indicates different parts of the model in 3D view. Fig. 3 shows the amplification mechanism of Bridge type amplifier.

2.1 Cad Model Of Mechanism Using Software

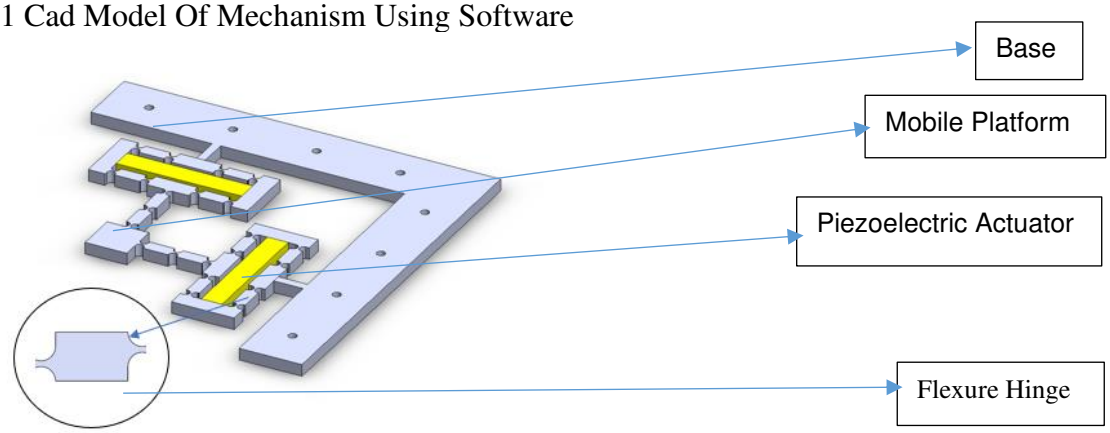


Fig 2: Monolithic 2-DOF micromanipulator model in 3D view.

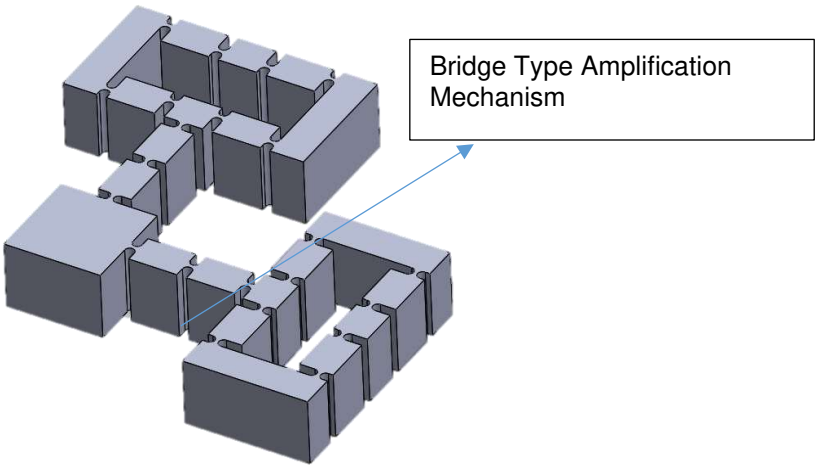


Fig 3: Kinematic chain of micromanipulator.

2.2 Mechanical Design Of 2-Dof Mechanism

Two bridge-type amplification mechanisms connected perpendicularly to flexure hinges built into an in-plane XY micropositioning stage make up this mechanism. When actuated, piezoelectric stacks transfer motion through the flexure-based kinematic chains to the mobile platform. A Piezoelectric actuator (SA050520) provides 31 μm stroke and 900 N force for the desired range and resolution. Right circular flexures are used with the best displacement accuracy and minimal parasitic motion. Fig. 4 illustrates the kinematic modelling for Bridge type amplification mechanism.

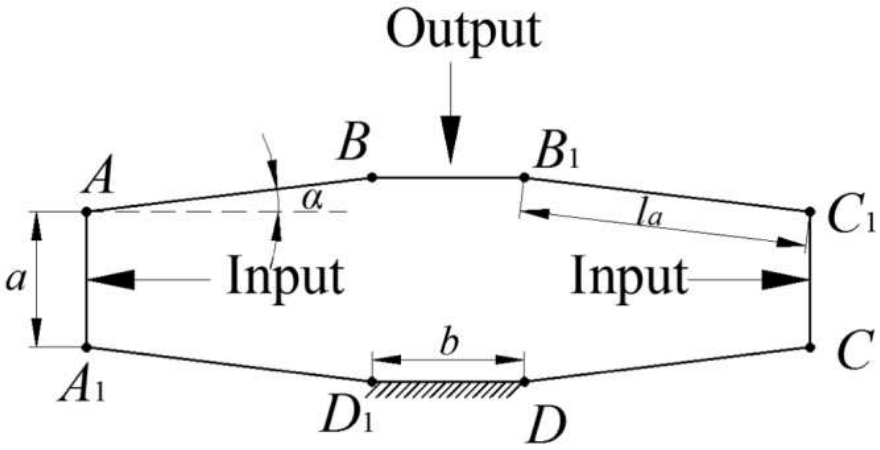


Fig 4: Bridge type amplification mechanism [39]

Equivalent compliance of flexure is,

$$C = \frac{9\pi r^{0.5}}{2Ebt^{2.5}} \qquad (1)$$

Where,
E= Young's modulus
w=Thickness
t= Critical thickness
r= Radius of circular flexure hinges
L= Distance between two adjacent hinge

2.3 Finite Element Analysis

FEA is employed to solve engineering challenges using software like ANSYS, which enables static, transient and dynamic simulation through modeling, optimization and analysis. ANSYS utilizes techniques such as static load steps, Newmark integration, and Newton-Raphson iteration to solve problems nonlinear equilibrium equations across load increments. Only relevant contact surfaces must be defined for penalty and Lagrange contact analysis in ANSYS. Finite Element Analysis of flexure-based mechanism has been shown in Fig. 5.

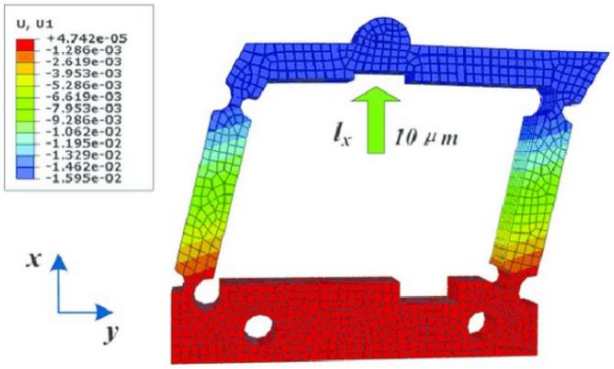


Fig. 5: Finite element method

2.4 Material Selection

The primary alloying component of the aluminum alloy 7075-T6 is zinc. Substantial flexibility, high strength, toughness, and exceptional fatigue resistance are just a few of its exceptional mechanical properties. It can produce motion in the micrometer range at the micro-level.

Table 1: Al 7075-T6's material properties

Properties	Values
Density	2810 kg/m3
Modulus of Elasticity	70.7 GPa
Poisson's Ratio	0.33
Bulk Modulus	70.29 GPa
Shear Modulus	26.955 GPa
Tensile Yield Strength	503 MPa
Compressive Yield Strength	503 MPa
Tensile Ultimate Strength	572 MPa
Shear Strength	333 MPa

2.5 Geometrical Model of The Micromanipulator

Fig. 6 demonstrates the geometrical modelling of the micromanipulator. It is required for calculating design parameters of the manipulator. Fig. 7 displays design of different shapes of flexure hinge and prismatic joints.

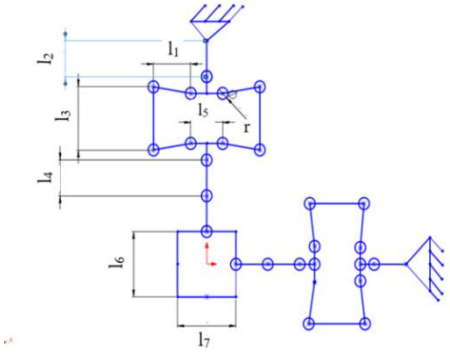


Fig. 6: Geometrical model of the micromanipulator.

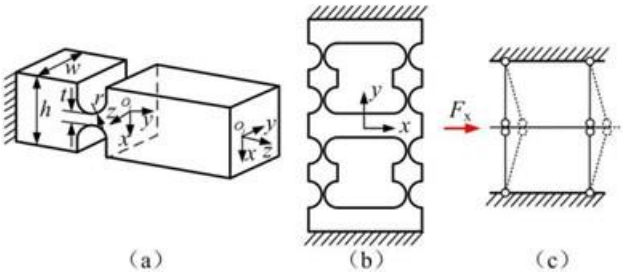


Fig. 7: (a) Design of flexure hinge. (b) Prismatic joint Joint [8]

Table 2: Design Parameters (mm)

l_1	l_2	l_3	l_4	l_5	l_6	l_7	r	t	b
7.01	5.98	10.60	6	6	11	11	1	0.4	6.5

2.6 Meshing

The 3D models drawn in SOLIDWORKS were meshed in ANSYS. The meshed models are shown in Fig 8 below. Its element size was 1 mm and Span Angle Center was Fine. Element number was 41041 and number of nodes was 203213. Fig. 8 demonstrates Meshing required for FEA.

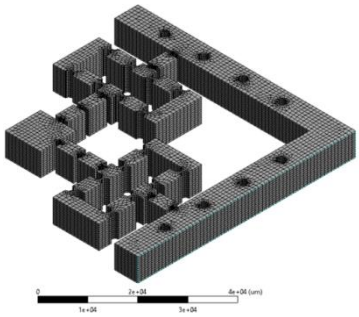


Fig 8: Mesh of the micromanipulator

2.7 Boundary Conditions

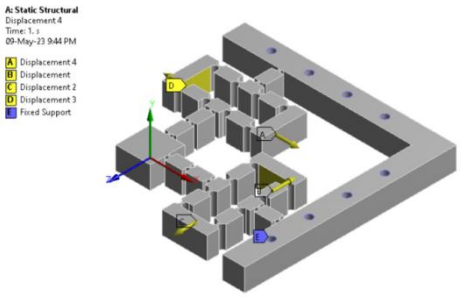


Fig 9: Boundary Condition Applied For Simulation.

Boundary condition is needed before simulation of this study. Necessary boundary condition was applied which is shown in Fig 9. Fixed support was applied in 8 holes in the base. Input displacement was applied in bridge type mechanism. Amount of input displacement along 2 direction was 31 µm in each bridge mechanism.

2.8 Selected Piezoelectric Actuator

Piezoelectric actuator model SA050520 was selected for this mechanism according to dimension and requirements. It has dimension of 5 mm×5 mm×20 mm. It operates voltage of 150V, capacitance 1.8 µm, stiffness 41 N/µm. It has input displacement range of 31 µm and force of 900 N.

3. RESULT AND DISCUSSION:

3.1 Displacement Amplification Ratio:

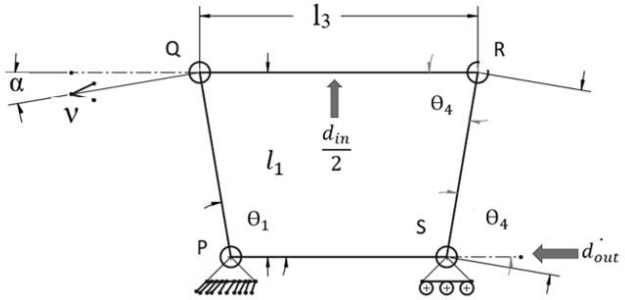


Fig. 10: Four-bar mechanism

Four bar mechanism has been implemented for analytical method which is illustrated in Fig. 10.

The P, Q, R, and S four-bar mechanism's geometric and motion relationships are taken into consideration. The linkage's relationship can be stated as follows:

$l_{PS}e^{i\Theta_1} = l_{PQ}e^{i\Theta_1} + l_{QR}e^{i\Theta_2} + l_{RS}e^{i\Theta_3}$ (4)

The following equations can be created using Eulers' formula to simplify Eq. (4) and then comparing the actual and imagined components from each side.

$l_{PS}sin\Theta_4 = l_{PQ}sin\Theta_1 + l_{QR}sin\Theta_2 + l_{RS}sin\Theta_3$ (5)

$l_{PS}cos\Theta_4 = l_{PQ}cos\Theta_1 + l_{QR}cos\Theta_2 + l_{RS}cos\Theta_3$ (6)

Differenting the Eqs. (5) and (6),

$\dot{d}_{out}cos\Theta_4 = l_{PQ}\omega_1 cos\Theta_1 + l_{QR}\omega_2 cos\Theta_2 + l_{RS}\omega_3 cos\Theta_3$ (7)

$\dot{d}_{out}\, sin\Theta_4 = l_{PQ}\omega_1 sin\Theta_1 + l_{QR}\omega_2 sin\Theta_2 + l_{RS}\omega_3 sin\Theta_3$ (8)

Substituting the ω_3 from Eq. (7) and (8)

$\dot{d}_{out} = -l_{PQ}\omega_1(cos\Theta_1 + \frac{sin\Theta_1}{l_{RS}sin\Theta_3}(l_{QR} + l_{RS}cos\Theta_3))$ (9)

Given by, v_1 is the tangential velocity at point Q.

$$v_1 = \omega_1 l_{PQ}$$

where $v_1 = \frac{\dot{d_{in}}}{2sin\alpha}$ and α = (90-Θ_1). Substituting $\omega_1$in Eq. (9), the displacement amplification ratio can be obtained as follows:

$r_{amp} = -\frac{1}{sin\alpha}\{cos\Theta_1 + \frac{sin\Theta_1}{l_{RS}sin\Theta_3}(l_{QR} + l_{RS}cos\Theta_3)\}$ (10)

From Eq. (12), r_{amp}= 6.77

3.2 Comparison of Amplification Ratio Between Analytical and FEA Method

Table 3: Comparison between analytical and FEA method

Input	Analytical	FEA	% of error
X	6.77	6.19	8.57%
Y	6.77	6.187	8.61%

3.3 Total Deformation

The total deformation of a flexure-based mechanism, including elastic deformation of flexure parts, is crucial for design and optimization. Excessive deformation can lead to malfunction, loss of accuracy, repeatability, and reliability. The total deformation of a mechanism was 194.96 μm, as

shown in Fig. 11.

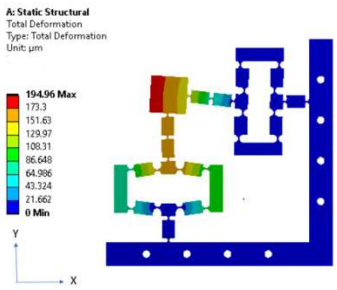


Fig 11: Total deformation

3.4 Equivalent (Von-Mises) Stress:

Equivalent von-Mises stress measures stress state in a flexure-based system, considering amplitude and distribution. It assesses fatigue life of the mechanism by estimating maximum stress endured by flexure elements during cyclic loading. The stress was calculated 297.64 MPa using FEA, as shown in Fig. 12.

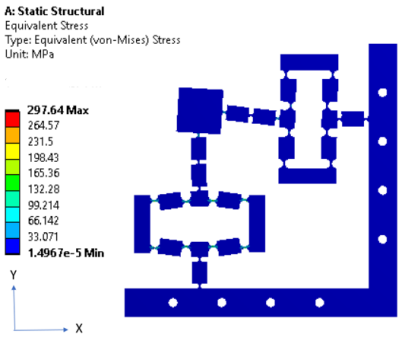
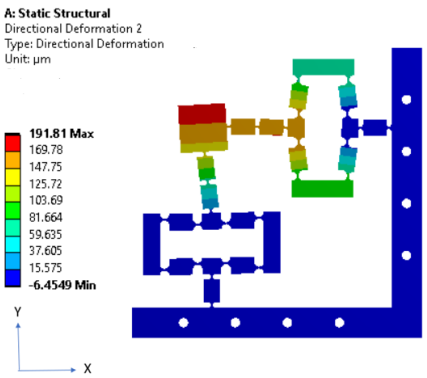
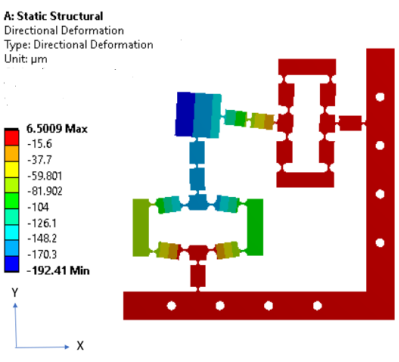


Fig. 12: Equivalent (von-Mises) stress

3.5 Directional Deformation:

Directional deformation in a flexure-based mechanism is crucial for achieving desired motion or force transmission. Engineers can optimize the design to reduce stress concentrations and improve accuracy and repeatability, ensuring the mechanism performs reliably over its intended lifespan. The micromanipulator's directional deformation along X and Y is 191.81 µm and 192.41 µm respectively in Fig. 13.





(a) (b)

Fig. 13: (a) Directional deformation along X axis (b) Directional deformation along Y axis

3.6 Input Displacement Vs Output Displacement And Amplification Ratio

Their geometry and mechanical characteristics influence the input and output displacements of circular flexures. For a given input displacement, the flexure's stiffness affects the output displacement. Stiffness increases with decreasing radius and thickness. Table 4 shows the variations in output displacement for various input displacement and amplification ratios. For a circular flexure with a radius of 1 mm, Fig. 14 shows the output displacement versus the input displacement. Input displacement is shown along the X-axis, and output displacement is shown along the Y-axis.

Table 4: Input Displacement, Output Displacement & Amplification Ratio

Input Displacement (µm)	Output Displacement (µm)	Amplification Ratio
5	31	6.2
10	62	6.2
15	94.33	6.2
20	125.78	6.2
25	157.22	6.2
30	188.67	6.2

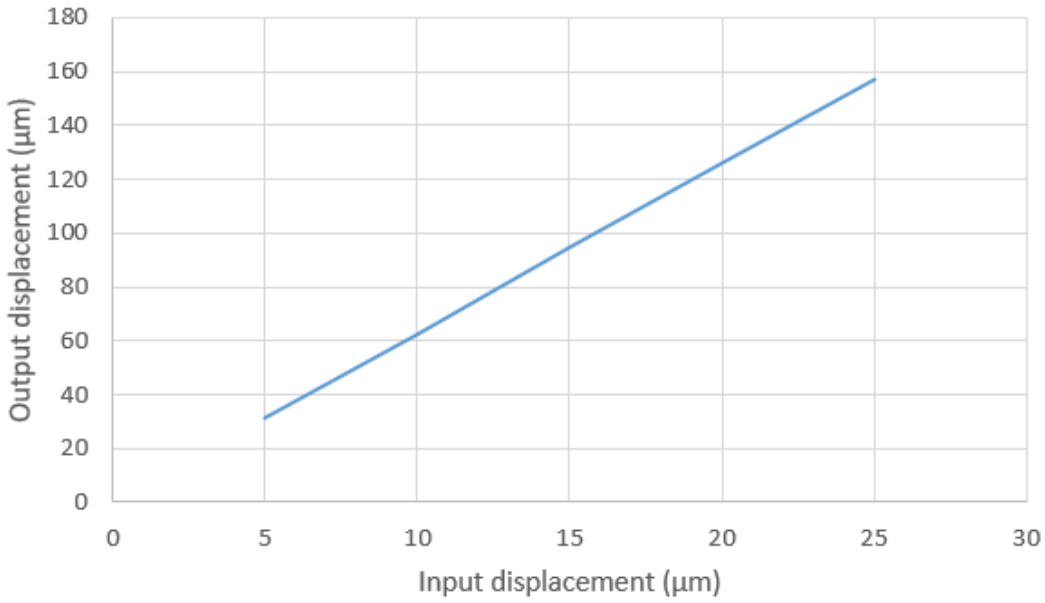


Fig. 14: Output Displacement Vs Input Displacement

3.7 Output Displacement Vs Input Displacement For Circular Flexure (Radius= 2mm)

Table 5 shows variation of output displacement for different input displacement and amplification ratio for circular flexure of radius 2 mm. Fig 15 represents output displacement vs input displacement for circular flexure of radius 2 mm. Along X axis, input displacement and Y axis, output displacement are represented.

Table 5: Input displacement, output displacement & amplification ratio

Input Displacement (µm)	Output Displacement (µm)	Amplification Ratio
5	27.43	5.49
10	54.86	5.49
15	82.29	5.49

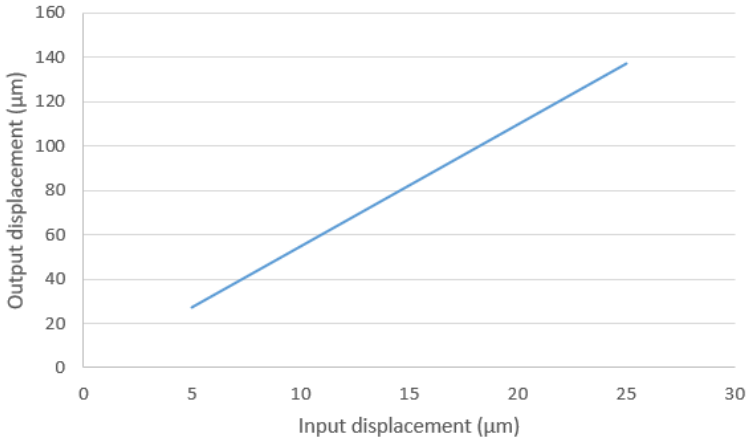
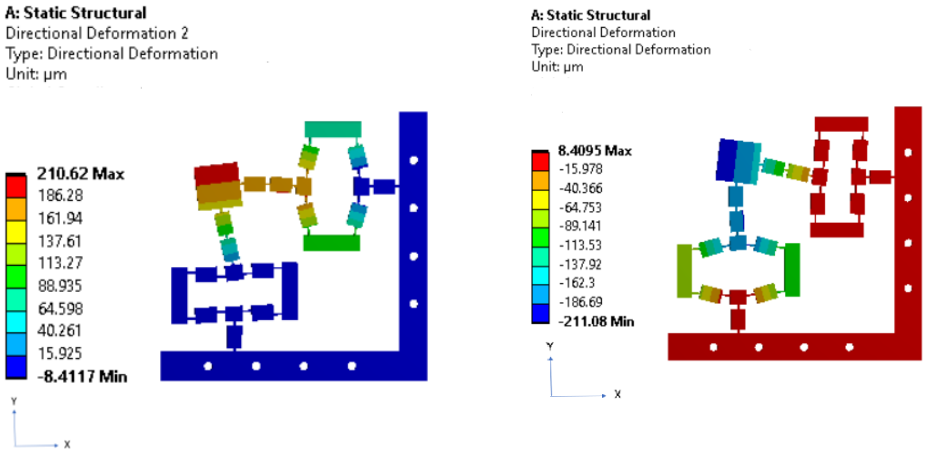


Fig 15: Output displacement vs Input displacement

From the above data, it was observed that as the radius of a circular flexure increased, output displacement, stiffness and amplification ratio were decreased.

3.8 FEA Analysis Using Leaf Flexure

Leaf flexures are a simple, high-strength flexure mechanism using thin, flat leaf springs for precise, repeatable motion or force transmission. They offer high precision, friction, and flexibility in motion direction and magnitude, making them a popular choice for applications. Directional deformation along X and Y axis for leaf flexure is shown in Fig. 16. It was found to be 210.62 µm and 211.08 µm respectively for input displacement of 31 µm .



(a) (b)

Fig. 16: Directional deformation for leaf flexure. (a) Directional deformation along X axis (b) Directional deformation along Y axis

Equivalent (von-Mises) for leaf flexure is shown in Fig. 17 Maximum stress was found from simulation by FEA was 125.58 MPa for input displacement of 31 µm

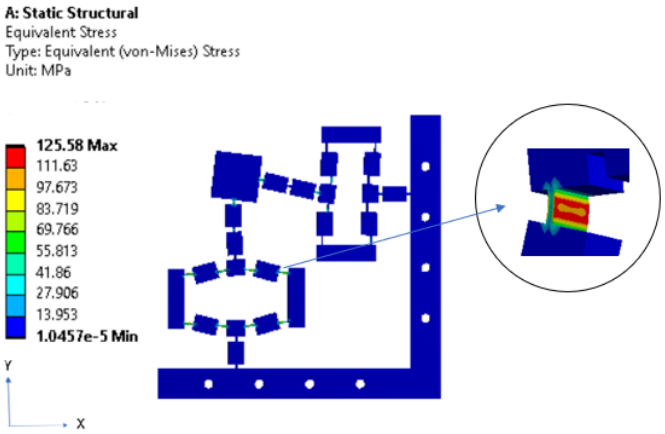


Fig. 18: Equivalent stress for leaf flexure

3.9 Output Displacement Vs Input Displacement For Leaf Flexure

Table 6 shows variation of output displacement for different input displacement and amplification ratio for leaf flexure. Fig 18 represents output displacement vs input displacement for leaf flexure. Along X axis, input displacement and along Y axis, output displacement are represented. It showed linear relationship between them.

Table 6: Input displacement, output displacement & amplification ratio

Input Displacement (µm)	Output Displacement (µm)	Amplification Ratio
5	34.44	6.89
10	68.89	6.89
15	103.33	6.89
20	137.77	6.89
25	172.22	6.89
30	206.66	6.89

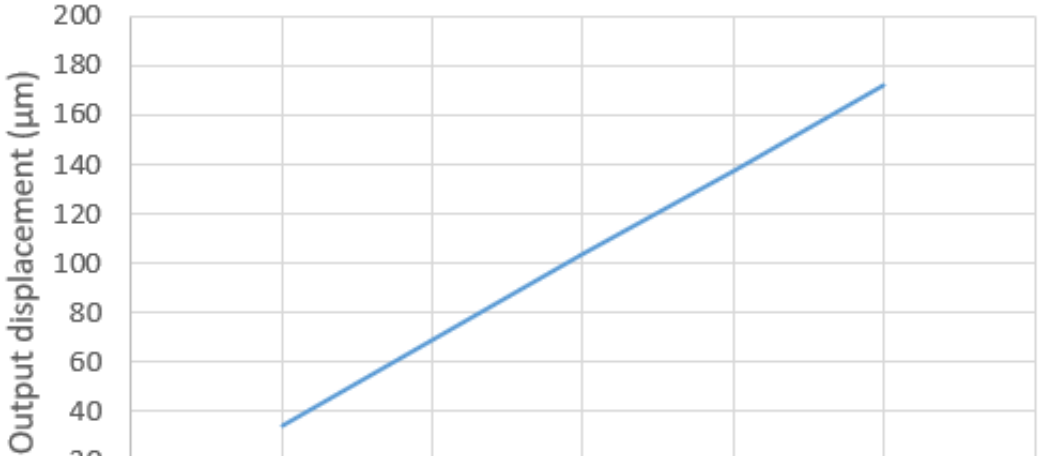


Fig. 19: Output Displacement Vs Input Displacement For Leaf Flexure.

3.10 Workspace

A 2 DOF flexure-based micromanipulator's workspace is the area that the end effector can access while it is moving in all directions. The geometry, mechanical characteristics, and actuator range all play a role in this. The output displacements can be calculated using the FEA model is.

$$\begin{bmatrix} X \\ Y \end{bmatrix} = \begin{bmatrix} J_{11} & J_{12} \\ J_{21} & J_{22} \end{bmatrix} \begin{bmatrix} d_{PEA1} \\ d_{PEA2} \end{bmatrix}$$

$$\Longrightarrow \begin{bmatrix} X \\ Y \end{bmatrix} = J_{com} \begin{bmatrix} d_{PEA1} \\ d_{PEA2} \end{bmatrix}$$

Jacobian matrix for workspace (2)

The input displacements from PEA1 and PEA2 are, respectively, dPEA1 and dPEA2. The appropriate output displacements of Motion Stage in the X and Y directions are represented by the letters X and Y, respectively. Jcom is the displacement amplification ratio for the designed mechanism's kinematic matrix.

By solving Jacobian matrix,

$$\begin{bmatrix} X \\ Y \end{bmatrix} = \begin{bmatrix} -6.16 & 0.027 \\ -0.085 & 6.219 \end{bmatrix} * \begin{bmatrix} 31 \\ 31 \end{bmatrix}$$

X = -190.12 µm, Y = 190.154 µm.

It depicts the movement of the motion stage along the X and Y axes when the input displacements for PEA1 and PEA2 were changed from 0 to 31 m.

The equation (2), which represents the quantity of input displacements in both bridge type mechanisms, was used to derive the inverse kinematics of this mechanism. A

$$\begin{bmatrix} dPEA1 \\ dPEA2 \end{bmatrix} = J'_{com} \begin{bmatrix} X \\ Y \end{bmatrix} \quad (3)$$

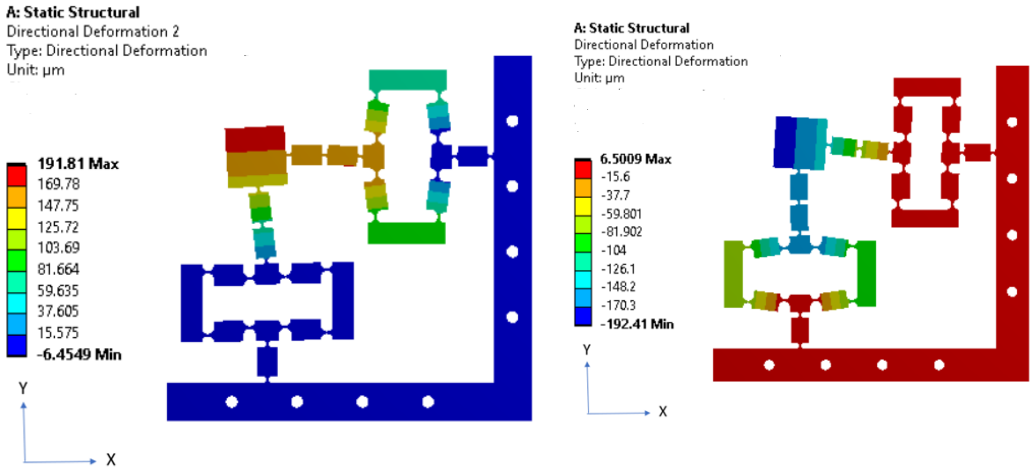
Here, J'_{com} is the inverse kinematic matrix representing displacement amplification ratio.

From Eq (3), the inverse kinematic matrix was, Eq (3),

$$J' = \begin{bmatrix} -0.1623 & 0.0007 \\ -0.0022 & 0.1608 \end{bmatrix}$$

3.11 Determination of Workspace using FEA

In Fig. 20 workspace was calculated. Along X direction it was found -191.81 µm and along Y direction it was found 192.41µm.



(a) (b)

Fig. 20: Workspace Using FEA, (a)Along X Direction It Was Found -191.81 µm (b)Along Y Direction It Was Found 192.41µm.

3.12 Rotaional Stiffness

$$\text{Rotational stiffness, } k_\theta = \frac{2Ebt^{2.5}}{9\pi R^{0.5}} \text{ [4]} \qquad (11)$$

From Eq. (11), $k_\theta = 104.17 \frac{N}{\mu m}$.

3.13 Dynamic Modelling

The natural frequency of the micromanipulator can be derived using the Lagrange equation:

$$\frac{d}{dt}\left(\frac{\partial T}{\partial q_i}\right) - \frac{\partial T}{\partial q_i} + \frac{\partial V}{\partial q_i} = F_i \qquad (12)$$

where the kinetic and potential energies of the mechanism are T and V, respectively, and is the generalized non-conservative force.

The motion of the linkage of the micromanipulator and piezoelectric actuation at the input ends of the mechanism's kinetic energy can be expressed as follows:

$$T = \frac{1}{2}m_A \dot{d}^2{}_{out} + \frac{1}{2}m_c\left\{\left(\frac{\dot{d_{in}}}{2}\right)^2 + \left(\frac{\dot{d_{out}}}{2}\right)^2\right\} \times 2 + \frac{1}{2}m_B\left\{\left(\frac{\dot{d_{in}}}{4}\right)^2 + \left(\frac{3\dot{d_{out}}}{4}\right)^2\right\} \times 4 +$$
$$\frac{1}{2}I_B \dot{\Theta_B}^2 \times 4 + \frac{1}{2}m_D\left\{\left(\frac{\dot{d_{in}}}{4}\right)^2 + \left(\frac{\dot{d_{out}}}{4}\right)^2\right\} \times 4 + \frac{1}{2}I_D \dot{\Theta}_D^2 \times 4 \qquad (12)$$

Where m_A, m_B, m_C, m_D are mass of the input end, the output end, and the connecting links as shown in Fig. I_B and I_D are the second moment of inertia of the mass of the link B and D. Substituting the $d_{out} = r_{amp} d_{in}$ and $\Theta_B = \Theta_D = \frac{d_{out}}{2L}$, the kinetic energy can be derived as,

T= $\frac{1}{2}m_A r_{amp}^2 \dot{d}^2{}_{in} + 2m_B\left(\frac{1}{16}+\frac{9}{16}r_{amp}^2\right)\dot{d}^2{}_{in} + \frac{1}{12}m_B r_{amp}^2 \dot{d}^2{}_{in} + m_c\left(\frac{1}{4}+\frac{1}{4}r_{amp}^2\right)\dot{d}^2{}_{in} + 2m_D\left(\frac{1}{16}+\frac{1}{16}r_{amp}^2\right)\dot{d}^2{}_{in}$ (13)

The potential energy of the mechanism due to elastic deformation of the flexure hinges can be expressed by:

$$V = 8 \times \frac{1}{2}k_\Theta(\Theta_B^2 + \Theta_D^2) \quad (14)$$

The equivalent mass and stiffness can be calculated by substituting the kinetic and potential energy equation from equations (15) and (16) into equation (13), as shown below.

$$M = m_A r_{amp}^2 + 4m_B\left(\frac{1}{16}+\frac{9}{16}r_{amp}^2\right) + \frac{1}{16}m_B r_{amp}^2 + 2m_c\left(\frac{1}{4}+\frac{1}{4}r_{amp}^2\right) + 4m_D\left(\frac{1}{16}+\frac{1}{16}r_{amp}^2\right)$$

$$K = \frac{4k_\Theta r_{amp}^2}{L^2} \quad [5] \quad (15)$$

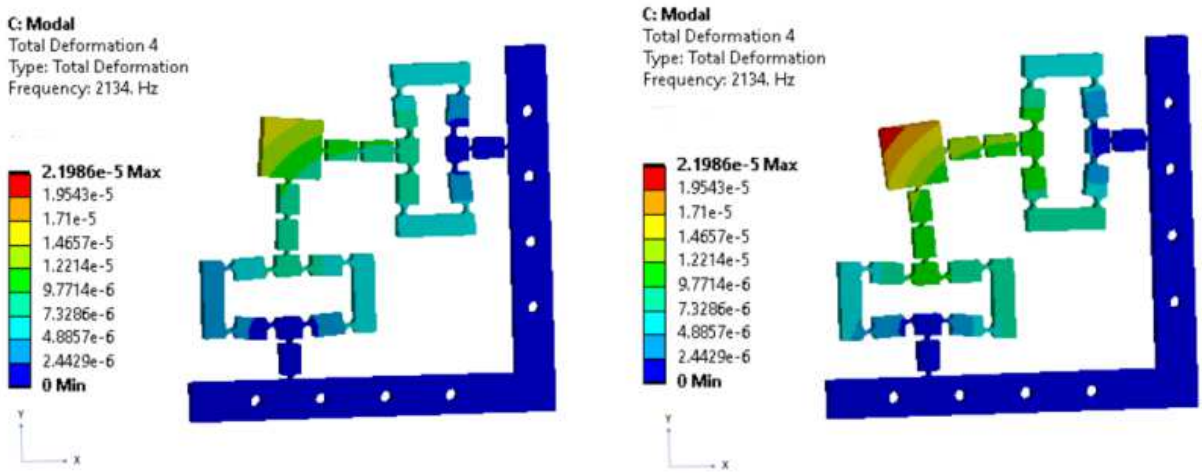
The natural frequency of the micromanipulator can be derived by:

$$f_n = \frac{1}{2\pi}\sqrt{\frac{K}{M}} \quad (16)$$

Equivalent mass, M = 0.200967 Kg.
Stiffness, K = 36.1 N/µm.
Natural frequency, f_n = 2133.10 Hz.

3.14 Modal Analysis

The equivalent mass and stiffness can be calculated by substituting the kinetic and potential energy equation from equations (15) and (16) into equation (13), as shown below. Two Mode shapes described two natural frequencies along two directions. Two mode shape are demonstrated in Fig. 21 Along both X and Y axis, natural frequency was found 2134 Hz which is close to analytical result of 2133 Hz.



(a) (b)

Fig. 21: Modal Analysis Of The Micromanipulator. (a) Natural Frequecy Along X Axis. (b) Natural Frequency Along Y Axis

Table 7: Comparison between analytical and FEA method

Input	Analytical	FEA	% of error
X	2133	2134	0.0468%
Y	2133	2134	0.0468%

3.15 Output Stiffness Of The Mechanism

Required reaction force calculating rotational stiffness has been displayed in Fig. 22.

Stiffness of the mechanism was calculated from,

$$F = k \times x \qquad (17)$$

Where, F = Reaction force of the motion stage, k = Output stiffness of the mechanism, x = Total deformation.

Output stiffness, $k = \frac{F}{x} = \frac{176.77}{237.71} = 0.74\ \mathrm{N/\mu m}$

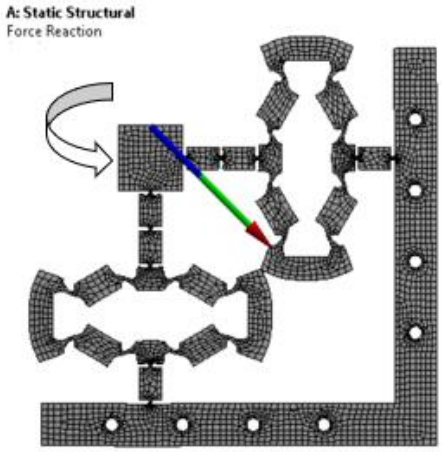


Fig. 22: Reaction Force Of The Mechanism

3.16 Safety Factor

The Safety Factor (FOS) is a safety margin in mechanical structure design, particularly in flexure-based mechanisms. It is calculated by comparing the material's ultimate strength to the applied load, determined through analytical or numerical methods like finite element analysis.

Safety factor $= \frac{Yield\ Strenth}{Tensile\ Strength} = \frac{503}{373.32} = 1.35$

3.17 Input Stiffness

$$k_{in} = \frac{2Ebt^3}{l(t^2\cos^2\theta + l^2\sin^2\theta)}\ [6] \qquad (18)$$

From Eq (18), input stiffness k_{in}= 6.2 N/µm.

Using FEA, the study examined the overall deformation of a 2-DOF mechanism with one mm-radius circular flexure. It was discovered that the output displacement was directly proportional to the input displacement and that the amplification ratio was 6.2. The calculated errors along X and Y were 8.57% and 8.61%, respectively. Workspace measurements along the X and Y axes were found to be -191.81 mm and 192.41 mm, respectively, and the output stiffness was 0.74 N/mm.

4. CONCLUSION

This study presented a 2-DOF parallel micromanipulator with natural frequency optimization, analyzed through computational analysis and modal testing. The mechanism showed good dynamic characteristics with a natural frequency of 2134 Hz and low percentage error. Amplification ratios

were calculated and validated through analytical and FEA methods. The output stiffness was 0.74 N/μm, and the safety factor was 1.35, which can be improved by optimizing the design. The study also explored the relationship between output and input displacement, which was found to be linear. Future works include parametric optimization, experimental studies, and the use of different actuators and techniques to enhance performance. The findings open up new possibilities for nanomanipulation and precision applications.

Declarations

Funding
(details of any funding received)
"Not applicable"

5. REFERENCES

[1] S. P. Jagtap, B. B. Deshmukh, and S. Pardeshi, "Applications of compliant mechanism in today's world – A review," J Phys Conf Ser, vol. 1969, no. 1, p. 012013, Jul. 2021.

[2] X. Jin, Y. Fang, D. Zhang, and J. Gong, "Design of dexterous hands based on parallel finger structures," Mech Mach Theory, vol. 152, p. 103952, Oct. 2020.

[3] J. Staley, D. Lege, J. T. Staley, and D. J. Lege, "Advances in aluminium alloy products for structural applications in transportation," Journal de Physique IV Proceedings, vol. 111, no. C7, p. 3, 1993.

[4] Yangmin Li and Qingsong Xu, "A novel design and analysis of a 2-DOF compliant parallel micromanipulator for nanomanipulation," IEEE Transactions on Automation Science and Engineering, vol. 3, no. 3, pp. 247–254, Jul. 2006.

[5] X. Xiao, Y. Li, and S. Xiao, "Development of a novel large stroke 2-DOF micromanipulator for micro/nano manipulation," Microsystem Technologies, vol. 23, no. 7, pp. 2993–3003, Jul. 2017.

[6] S. M. Berry, S. A. Harfenist, R. W. Cohn, and R. S. Keynton, "Characterization of micromanipulator-controlled dry spinning of micro- and sub-microscale polymer fibers," Journal of Micromechanics and Microengineering, vol. 16, no. 9, pp. 1825–1832, Sep. 2006.

[7] S. Awtar, "Synthesis and Analysis of Parallel Kinematic XY Flexure Mechanisms," 1998.

[8] H. Tang, Y. Li, J. Huang, and Q. Yang, "Design and assessment of a flexure-based 2-DOF micromanipulator for automatic cell micro-injection," in Advanced Materials Research, 2012, pp. 445–448.

[9] I. Q. Meng, G. Berselli, and R. Vertechy, "A Design Method for Flexure-Based Com-pliant Mechanisms on the Basis of Stiffness and Stress Characteristics."

[10] K. Q. Qi, Y. Xiang, C. Fang, Y. Zhang, and C. S. Yu, "Analysis of the displacement amplification ratio of bridge-type mechanism," Mech Mach Theory, vol. 87, pp. 45–56, 2015.

[11] K. A. Jensen, C. P. Lusk, and L. L. Howell, "An XYZ Micromanipulator with three translational degrees of freedom," Robotica, vol. 24, no. 3, pp. 305–314, May 2006.

[12] Y. L. Zhang, M. L. Han, M. Y. Yu, C. Y. Shee, and W. T. Ang, "Automatic hysteresis modeling of piezoelectric micromanipulator in vision-guided micromanipulation systems," IEEE/ASME Transactions on Mechatronics, vol. 17, no. 3, pp. 547–553, 2012.

[13] Y. Li, J. Huang, and H. Tang, "A compliant parallel XY micromotion stage with complete kinematic decoupling," IEEE Transactions on Automation Science and Engineering, vol. 9, no. 3, pp. 538–553, 2012.

[14] Y. Li and Q. Xu, "Optimal Design of a Novel 2-DOF Compliant Parallel Micromanipulator for Nanomanipulation."

[15] Y. Li and Q. Xu, "Design and optimization of an XYZ parallel micromanipulator with flexure hinges," Journal of Intelligent and Robotic Systems: Theory and Applications, vol. 55, no. 4–5, pp. 377–402, 2009.

[16] J. Pinskier, B. Shirinzadeh, L. Clark, and Y. Qin, “Development of a Dexterous Haptic Micro/Nanomanipulator Utilizing a Hybrid Parallel-Serial Flexure Mechanism.”
[17] Y. Qin, B. Shirinzadeh, Y. Tian, D. Zhang, and U. Bhagat, “Design and computational optimization of a decoupled 2-DOF monolithic mechanism,” IEEE/ASME Transactions on Mechatronics, vol. 19, no. 3, pp. 872–881, 2014.
[18] J. Wu, J. Wang, T. Li, and L. Wang, “Analysis and application of a 2-DOF planar parallel mechanism,” Journal of Mechanical Design, Transactions of the ASME, vol. 129, no. 4, pp. 434–437, Apr. 2007.
[19] Y. Li and Q. Xu, “Modeling and performance evaluation of a flexure-based XY parallel micromanipulator,” Mech Mach Theory, vol. 44, no. 12, pp. 2127–2152, 2009.
[20] Y. Tian, B. Shirinzadeh, D. Zhang, X. Liu, and D. Chetwynd, “Design and forward kinematics of the compliant micro-manipulator with lever mechanisms,” Precis Eng, vol. 33, no. 4, pp. 466–475, Oct. 2009.
[21] J. A. Saglia, N. G. Tsagarakis, J. S. Dai, and D. G. Caldwell, “A high-performance redundantly actuated parallel mechanism for ankle rehabilitation,” International Journal of Robotics Research, vol. 28, no. 9, pp. 1216–1227, Sep. 2009.
[22] N. Ashida et al., “Isolation of functional single cells from environments using a micromanipulator: Application to study denitrifying bacteria,” Appl Microbiol Biotechnol, vol. 85, no. 4, pp. 1211–1217, Jan. 2010.
[23] E. G. Merriam, J. E. Jones, S. P. Magleby, and L. L. Howell, “Monolithic 2 DOF fully compliant space pointing mechanism,” Mechanical Sciences, vol. 4, no. 2, pp. 381–390, 2013.
[24] S. C. Huang and T. P. Dao, “Multi-objective Optimal Design of a 2-DOF Flexure-Based Mechanism Using Hybrid Approach of Grey-Taguchi Coupled Response Surface Methodology and Entropy Measurement,” Arab J Sci Eng, vol. 41, no. 12, pp. 5215–5231, Dec. 2016.
[25] L. Clark, B. Shirinzadeh, J. Pinskier, Y. Tian, and D. Zhang, “Topology optimisation of bridge input structures with maximal amplification for design of flexure mechanisms,” Mech Mach Theory, vol. 122, pp. 113–131, Apr. 2018.
[26] N. Ma, J. Yu, X. Dong, and D. Axinte, “Design and stiffness analysis of a class of 2-DoF tendon driven parallel kinematics mechanism,” Mech Mach Theory, vol. 129, pp. 202–217, Nov. 2018.
[27] Z. Wu et al., “Tracking Control of PZT-Driven Compliant Precision Positioning Micromanipulator,” IEEE Access, vol. 8, pp. 126477–126487, 2020.
[28] Q. Xu, Y. Li, and N. Xi, “Design, fabrication, and visual servo control of an xy parallel micromanipulator with piezo-actuation,” IEEE Transactions on Automation Science and Engineering, vol. 6, no. 4, pp. 710–719, 2009.
[29] F. Wang, B. Shi, Y. Tian, Z. Huo, X. Zhao, and D. Zhang, “Design of a Novel Dual-Axis Micromanipulator with an Asymmetric Compliant Structure,” IEEE/ASME Transactions on Mechatronics, vol. 24, no. 2, pp. 656–665, Apr. 2019.
[30] X. Sun et al., “Design and analysis of a large-range precision micromanipulator,” Smart Mater Struct, vol. 28, no. 11, Oct. 2019.
[31] A. Sharon Neville Hogan and D. E. Hardt, “HIGH BANDWIDTEI FORCE REGULATION AND INERTIA REDUCTION USING A MACRO/HICRO MANIPULATOR SYSTEM.”
[32] A. Al-Jodah et al., “Modeling and a cross-coupling compensation control methodology of a large range 3-DOF micropositioner with low parasitic motions,” Mech Mach Theory, vol. 162, Aug. 2021.
[33] J. Lin, C. Qi, F. Gao, Y. Yue, Y. Hu, and B. Wei, “Modeling and Verification for a Three-Degree-of-Freedom Flexure-Based Planar Parallel Micro Manipulator,” J Mech Robot, vol. 15, no. 4, Aug. 2023.
[34] Y. Li and Q. Xu, “Optimal Design of a Novel 2-DOF Compliant Parallel Micromanipulator for Nanomanipulation.”
[35] Y. Liu, “ANSYS and LS-DYNA used for structural analysis,” International Journal of Computer Aided Engineering and Technology, vol. 1, no. 1, pp. 31–44, 2008.

[36] Y. Tian, B. Shirinzadeh, and D. Zhang, “Design and dynamics of a 3-DOF flexure-based parallel mechanism for micro/nano manipulation,” Microelectron Eng, vol. 87, no. 2, pp. 230–241, Feb. 2010.
[37] IEEE Nanotechnology Council, Guo jia zi ran ke xue ji jin wei yuan hui (China), and Institute of Electrical and Electronics Engineers, Conference program digest : the 7th International Conference on Manipulation, Manufacturing and Measurement on the Nanoscale : IEEE 3M-NANO 2017 : Shanghai, China, 7-11 August 2017.
[38] https://www.smithsadvanced.com/ (DOA: 24 March, 2023)
[39] P .Liu and P. Yan, “A new model analysis approach for bridge-type amplifiers supporting nano-stage design,” Mech Mach Theory, vol. 99, pp. 176–188, May 2016.